

# Human-robot collaborative assembly of movable airfoils using adaptive admittance control

Ye Shen

*College of Mechanical and Electrical Engineering, NUAU, Nanjing, China*

Bo Li

*College of Mechanical and Electrical Engineering, NUAU, Nanjing, China and Jiangsu Key Laboratory of Precision and Micro-Manufacturing Technology, NUAU, Nanjing, China, and*

Wei Tian, Jinjun Duan and Mingxuan Liu

*College of Mechanical and Electrical Engineering, NUAU, Nanjing, China*

## Abstract

**Purpose** – With the increasing requirements for intelligence in the field of aviation manufacturing, manual assembly can hardly adapt to the trend of future production. The purpose of this study is to realize the semi-automatic assembly of the movable airfoil by proposing a human-robot collaborative assembly strategy based on adaptive admittance control.

**Design/methodology/approach** – A logical judgment system for operating intentions is introduced in terms of different situations of the movements; hence, a human cognition-based adaptive admittance control method is developed to curb the damage of inertia; then virtual limit walls are raised on the periphery of the control model to ensure safety; finally, simulated and experimental comparisons with other admittance control methods are conducted to validate the proposed method.

**Findings** – The proposed method can save at least 28.8% of the time in the stopping phase which effectively compensates for inertia during the assembly process and has high robustness concerning data disturbances.

**Originality/value** – Due to the human-robot collaboration to achieve compliant assembly of movable airfoils can preserve human subjectivity while overcoming the physical limits of humans, which is of great significance to the investigation of intelligent aircraft assembly, the proposed method that reflects the user's naturalness and intuitiveness can not only enhance the stability and the flexibility of the manipulation, but also contribute to applications of industrial robots in the field of human-robot collaboration.

**Keywords** Adaptive admittance control, Human-robot collaboration, Aircraft assembly, Industrial robotics, User-friendliness

**Paper type** Research paper

## 1. Introduction

As a strategic industry, the aviation industry plays an important role in guaranteeing the economy, technology and national defense construction (Li *et al.*, 2022). As for aircraft fabrication, the assembly workload generally accounts for 50–70% of that of the whole manufacturing, which renders it the most important aspect (Pérez *et al.*, 2020). However, the current assembly of aviation equipment usually relies on manual operation, which is labor-



intensive and inefficient, making it difficult to adapt to the trend of future production. To achieve flexible manipulation of movable airfoils, the human-robot interaction (HRI) strategy, where the combination of mechanical strength of a robot and subjectivity of a human can make the human-robot system superior to a robot or an individual human, is of great significance to the investigation of intelligent aircraft assembly.

One of the key roles of the robot is to add the required operating force to overcome the physical limits of humans, thus the introduction of industrial robots with greater load-bearing capacity into the HRI field can provide more physical assistance to humans (Peng *et al.*, 2021). However, the explorations of human-robot collaborative assembly are mostly focused on lightweight objects (Cherubini *et al.*, 2016; Lv *et al.*, 2022), which is relatively absent on heavy objects using large industrial robots. Considering the phenomenon of the device for heavy workpieces that may move involuntarily without any operating force due to incorrect inertia and gravity compensation, the safety and reliability of the HRI and performance should be rigorously tested while providing greater capabilities like strength, speed and accuracy (Yang *et al.*, 2021).

Compliant control, as a vital link in formulating control rules in HRI, is essential to coordinate the relationship between human operators and robots aiming to achieve consensus in the interaction process. According to the different modeling methods, compliant control can be divided into hybrid position/force control (Rojas-García *et al.*, 2022), impedance control (Farhadiyadkuri *et al.*, 2022) and admittance control mainly, where the hybrid position/force control requires frequent transitions of force-control or position-control which is barely suitable for the unstructured complex environment in this subject. The application of impedance control is also limited for the inaccessible to obtain an accurate impedance control model due to its complex dynamics modeling process. Hence, the admittance control with the advantages of being hardly affected by environmental or robot dynamics modeling factors is appropriate for the research.

Tsumugiwa *et al.* (2017) investigated a variable admittance control of the robot at low speed ( $\leq 0.02$  m/s), which performed significantly compared to the fixed admittance control; however, the method was only applicable to low-speed conditions, which limited its application. Akgun *et al.* (2020) estimated the user-applied force to perform adaptive impedance control by parameter identification of a four-bar mechanism. Although the usage of force sensors was omitted, due to the dynamics model for a 6-DOF robot being tougher to obtain as well as the fact that the model was prone to varying with different objects, the versatility of the solution is deficient. Wu *et al.* (2021) proposed a variable admittance control method based on human intentions, which rendered the robot to respond to the human operator safely, whereas the large inertia presented in the load during the compliant assembly is not considered. Kim (2022) introduced a sensorless admittance control of a 3-DOF manipulator for collision detection, though the method avoids the usage of force sensors, its application in 6-DOF robots is less practical owing to the difficulty to obtain the robot dynamics model, besides the model is prone to change with the replacement of the end load.

Thus, the core innovations we attempt to bring are: (1) proposing user-friendly control strategies for the compliant assembly of the movable airfoil in terms of human cognition, (2) illustrating approaches to select coefficients with consideration of system stability and large inertia and (3) developing virtual walls to limit the manipulating region in views of security risks. Finally, the simulated and experimental validation approaches are generated to verify the effectiveness of the proposed method compared with other admittance methods.

## 2. Adaptive admittance control model

The movable airfoils are characterized by large volume and weight with poor rigidity, so the chattering of the load may affect force perception and lead to system chattering, making them less stable in resisting the transformations of motion states. Therefore, to avoid the collision hazards caused by the sliding of robot arms or the instability of the device being amplified, it is crucial to restrain the inertia in the collaborative assembly of the movable airfoil.

Admittance control is generally represented by a classical model of a second-order differential equation, namely, the “mass-damping-spring” model, as shown in Figure 1.

According to the model, the admittance equation of the industrial robot can be expressed as follows:

$$f_{Hj} = m_j(\ddot{x}_j - \ddot{x}_{dj}) + b_j(\dot{x}_j - \dot{x}_{dj}) + k_j(x_j - x_{dj}) \quad (1)$$

where  $j = 1-6$ ,  $f_{Hj}$  represents the interaction force/torque in each dimension;  $m_j$  and  $b_j$ , respectively, represent the virtual mass and the virtual damping of each dimension, while  $k_j$  representing the virtual stiffness.  $\ddot{x}_j$ ,  $\dot{x}_j$  and  $x_j$  represent the acceleration, velocity and displacement of the robot end in each dimension, respectively, and the subscript  $d$  corresponds to the desired value of each parameter.

Since the dragging action normally has no constraints, and there are no preset trajectory bindings, the virtual stiffness  $k_j$  and the desired acceleration  $\ddot{x}_{dj}$ , desired velocity  $\dot{x}_{dj}$  and desired displacement  $x_{dj}$  can be set to zero. Then the admittance equation (1) can be simplified as

$$f_{Hj} = m_j\ddot{x}_j + b_j\dot{x}_j \quad (2)$$

Taking the Laplace transform of (2), the model behaves as an integrator in the position domain and a first-order transfer function in the velocity domain for the interaction force/torque as the step input to the system.

$$\dot{X}_j(s) = \frac{F_{Hj}(s)}{m_j s + b_j} = \frac{F_H(s)/b_j}{\frac{m_j}{b_j} s + 1} = F_{Hj}(s)H_j(s) \quad (3)$$

where  $\dot{X}_j(s)$  and  $F_{Hj}(s)$  represent the Laplace transforms of  $\dot{x}_j$  and  $f_{Hj}$ , respectively, and  $H_j(s)$  is the transfer equation.

Due to the destination of dragging being random, whereas the velocity vector can be calculated, the displacement of the robot end can be eventually acquired by integrating the velocity. After treating (2) with a zero-order holder, the theoretical discretization velocity can be obtained as

$$\dot{x}_{thj}(k) = \frac{f_{Hj}(k) - b_j\dot{x}_{thj}(k-1)}{m_j} T_s + \dot{x}_{thj}(k-1) \quad (4)$$

where  $f_{Hj}(k)$  represents the interaction force at time  $k$ ;  $\dot{x}_{thj}(k-1)$  and  $\dot{x}_{thj}(k)$  represent the theoretical velocity at time  $k-1$  and  $k$  separately;  $T_s$  is the sampling period. Given the connection between motion parameters, the theoretical acceleration and displacement can be expressed as follows:

$$\begin{aligned} \ddot{x}_{thi}(k) &= \frac{f_{Hi}(k) - b_i\dot{x}_{thi}(k-1)}{m_i} \\ x_{thi}(k) &= \frac{f_{Hi}(k) - b_i\dot{x}_{thi}(k-1)}{m_i} T_s^2 + \dot{x}_{thi}(k-1)T_s + x_{thi}(k-1) \end{aligned} \quad (5)$$

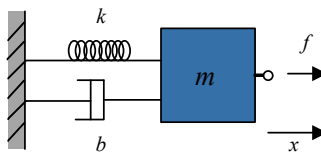


Figure 1. Schematic of mass-damping-spring model

where  $\ddot{x}_{thi}(k)$  represents the theoretical acceleration at time  $k$ ,  $x_{thi}(k-1)$  and  $x_{thi}(k)$  represent the theoretical displacement at time  $k-1$  and  $k$  separately. Therefore, the control scheme in this work is determined in Figure 2.

To form user-friendliness between the robot and human operators, the coefficients  $m$  and  $b$  should be determined properly, Equation (3) has revealed that the virtual damping  $b$  can affect the steady-state of the response while the ratio  $m/b$  affects the system dynamics. And in (4), the velocity is a coupling between the mass factor  $m$  and the damping factor  $b$ .

2.1 Logic judgment of operating intentions

Normally, the motion can be classified into two cases: acceleration and deceleration. The former can be divided into two scenarios, one is to break the robot’s stationary state to have acceleration in a certain direction, and the other refers to the scenario in which the velocity direction coincides with the acceleration direction during the robot’s movement. The latter generally refers to the scenario in which the velocity direction is opposite to the acceleration direction during the movement.

However, considering the large weight and weak rigidity of the workpieces in this work, the entire process cannot be satisfied by only two cases, thus four cases are nominated to describe operating intentions as acceleration, deceleration, stopping and quiescence. The acceleration is consistent with the previous scenarios, whereas the deceleration happens in the presence of an external force applied by humans compared with the preceding scenario. The stopping case refers to the scenario in which the robot decreases its speed or even reaches

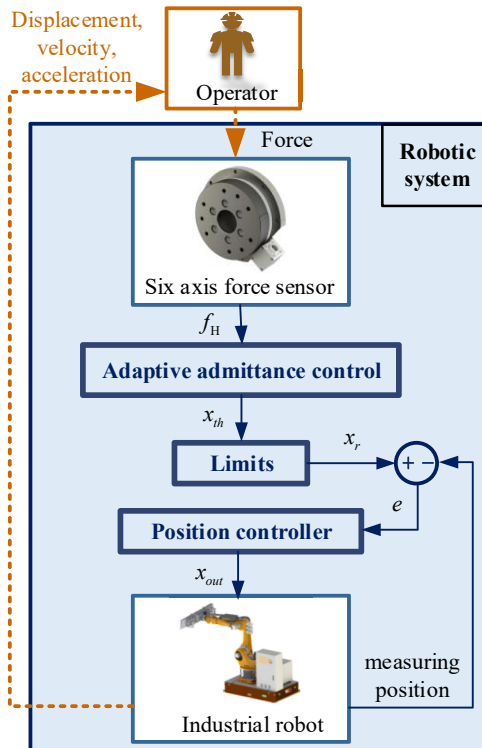


Figure 2. The control scheme of the assembly system

a stationary state after the external force is withdrawn, which expects the robot to stop quickly due to the concern for risk avoidance cause the exercise of the industry robot is unavailable to be controlled by human operators. The quiescent case refers to the state in which the force, velocity and acceleration are all zero. Therefore, the logic identification of the operating intentions in this section is mainly based on three dimensions of force, velocity and acceleration; the specific logic judgment is shown in Figure 3, which can be declared as: (1) if  $\ddot{x}_b \neq 0$  and  $\ddot{x}_b \cdot \dot{x}_b \geq 0$ , the operating intention is acceleration, (2) if  $\ddot{x}_b = \dot{x}_b = 0$ , the operating intention is quiescence. Then in the rest scenarios, (3) if  $f_H \neq 0$ , the operating intention is deceleration, (4) if  $f_H = 0$ , the operating intention is stopping.  $\dot{x}_b$  and  $\ddot{x}_b$ , respectively, represent the velocity and the acceleration at the last sampling moment of the robot end, and  $f_H$  indicates the interaction force/torque applied by human operators.

2.2 Online adjustments of the admittance coefficients

Since mobility and stability are two important metrics during a motion, the adjustments of the admittance coefficients should take them into account. It has been recognized that virtual damping has a greater effect on human perception than the virtual mass in the admittance control (Bian et al., 2020); however, the performances of the two coefficients are a consistent tendency. Low admittance coefficients (including virtual damping and virtual mass) require less interaction force to accelerate the robot which results in low fatigue, but the precision and the stability in manipulation may reduce due to the reason that the robot is more reactive. On the contrary, high admittance coefficients may lead to a less mobile but more stable condition. Obviously, there is a dynamic balance between the two capabilities, which also causes the main drawback of the fixed-conductance control method.

Considering the peculiarities of the HRI and performance, where the immeasurable human factor is included in the control loop, it is difficult to describe the stability of the system mathematically, while the experimental phenomenon of trembling can provide a reference. We found that when the virtual damping is set at a low value, the inflexible behavior of human operators may cause a significant trembling of the robot, hence the occurrence of trembling can be defined as system instability, otherwise be considered as stability. Then an experimental calibration diagram distinguishing the stable and unstable regions of admittance coefficients is illustrated in Figure 4.

The demarcation line in Figure 4 is noted as the calibration line. Then the area below the line indicates the unstable region where trembling will occur, while the area above indicates the stable region. Known from (3), the virtual damping  $b$  and the ratio  $m/b$  will affect the

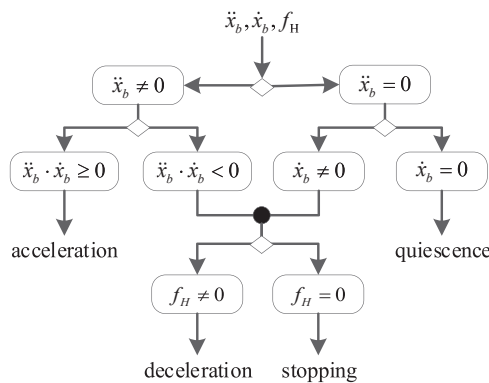
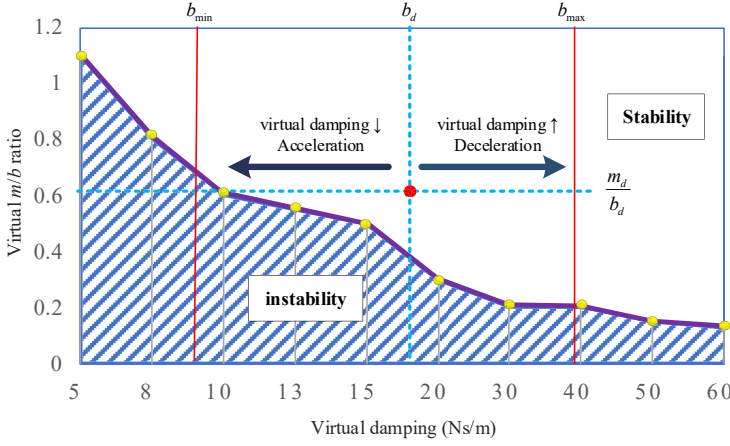


Figure 3. Operating intention logic judgment chart



**Figure 4.** Experimental calibration diagram of admittance coefficients

dynamics of the system, which reflected in Figure 4 is that the closer the selected virtual damping is to the vertical axis, the faster the robot moves with a larger instability proportion. Therefore, to achieve the user-friendliness of HRI and performance, virtual damping should be regulated in combination with human cognition.

First, initial damping ought to be selected in Figure 4 to locate the quiescence state. Then, for the intention to accelerate, the virtual damping locates to the left of the initial damping and decreases as the acceleration increases; otherwise, the virtual damping locates to the right of the initial damping and increases as the acceleration increases. And the distinction between the deceleration and the stopping status is that the latter owns a higher decreasing acceleration. Thus, the laws can be obtained as follows:

$$b_v = \begin{cases} b_d & \text{quiescence} \\ \max(b_d - \lambda_1 |\ddot{x}_b|, b'_{\min}) & \text{acceleration} \\ \min(b_d + \lambda_2 |\ddot{x}_b|, b'_{\max}) & \text{deceleration} \\ b_d + \lambda_2 |\ddot{x}_b| & \text{stopping} \end{cases} \quad (6)$$

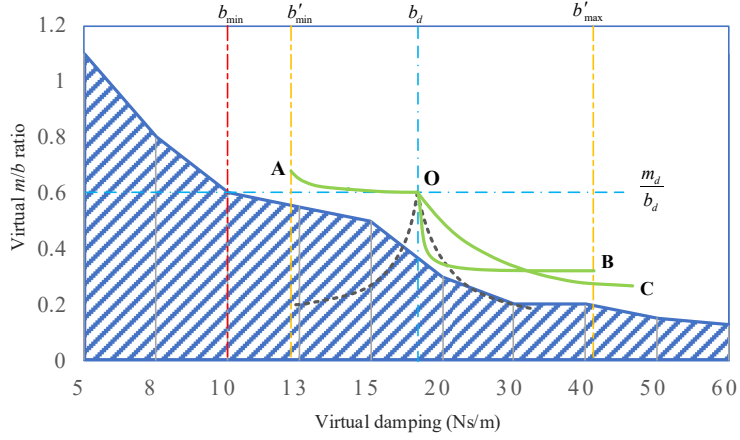
where  $b_v$  represents the controllable virtual damping and  $b_d$  represents the initial virtual damping set in the quiescence state. To avoid the coefficients falling into the unstable region, the maximum variation region of the virtual damping value is defined in the calibration diagram in this paper, which is noted as  $[b_{\min}, b_{\max}]$ .  $\lambda_1$  and  $\lambda_2$  in (6) are the parameters to adjust the change rate and change range of the virtual damping, which can be roughly estimated by

$$\begin{cases} \lambda_1 \approx \frac{b_d - b_{\min}}{|\ddot{x}|_{\max}} \\ \lambda_2 \approx \frac{b_{\max} - b_d}{|\ddot{x}|_{\max}} \end{cases} \quad (7)$$

where  $|\ddot{x}|_{\max}$  is the maximum acceleration set based on the specific demand of the system.

For the closer the admittance coefficient is to the lower-left corner in Figure 4, the more reactive the robot behaves, the trends of the ideal coefficient variations are expected as the dashed lines shown in Figure 5. However, the tendency can lead the admittance coefficients to

**Figure 5.**  
Design of the  
admittance coefficient  
regulation



enter the unstable region facily, consequently, the modified trends are expressed by the solid lines in Figure 5.

The initial admittance coefficients can be denoted at point O in Figure 5, which indicates the quiescence state. Then, when the human operator tends to accelerate the object, the coefficients are desired to vary along the edge of the unstable region, as shown by the OA line. And when the operator tends to decelerate, the curve for the coefficients ought to adapt to the decay tendency of the unstable region, as shown by the OB line. Therefore, a maximum range of the admittance coefficients should be limited to prevent the mutation during the reverse acceleration phase. Finally, when the robot is in the stopping case, to achieve a faster but smooth stop, the coefficients are considered to vary as the OC line. Hence, the strategy for the virtual mass can be constructed as follows:

$$m_v = \begin{cases} m_d & \text{quiescence} \\ b_v m_d / b_d + \Gamma & \text{acceleration} \\ b_v m_d \cdot \Lambda / b_d & \text{deceleration} \\ m_0 & \text{stopping} \end{cases} \quad (8)$$

where  $m_v$  represents the controllable virtual mass,  $m_d$  represents the initial virtual mass and  $m_0$  represents the virtual mass set in the stopping state.  $\Gamma$  and  $\Lambda$  are introduced to regulate the trend of the OA line and OB line, respectively, whose mathematical expressions can be chosen as follows:

$$\Gamma = e^{\beta \cdot (|x| - |x|_{\max})} \quad (9)$$

$$\Lambda = 1 - \alpha(1 - e^{-\varphi(b_v - b_d)}) \quad (10)$$

where  $\beta$  is to optimize the steepness of the OA line,  $\alpha$  is to manage the descent degree of the OB line to avoid the coefficients accessing the instability region, and  $\varphi$  is to adjust the convergence degree of the OB line.

### 3. Manipulation limited virtual walls

Since the industrial robot is released from its physical “cage”, natural or unintended human actions may cause serious consequences. Besides, the heavy load environment of the movable

airfoil assembly tends to destabilize the entire hardware system in certain robot poses, which also expands the unstable region in Figure 4 and even the risk of capsizing. Accordingly, the limitation of the robot's manipulating space should be considered.

In view of the failure of the physical passive isolation, virtual walls are created in this paper based on the correlation between the force and the position to limit the robot's manipulating space, which is separated into an inner wall and an outer wall, as shown in Figure 6.

When the movement of the robot end happens within the inner wall, there exist no restrictions, so the robot can interact normally. The actual displacements can be expressed as follows:

$$\begin{cases} x_{aci}(k) = x_{thi}(k) \\ \theta_{aci}(k) = \theta_{thi}(k) \end{cases} \quad (11)$$

where  $i = 1-3$ ,  $x_{aci}(k)$  and  $\theta_{aci}(k)$  represent the actual displacements of the robot end in position space and posture space at moment  $k$ , respectively.

However, when the robot end moves beyond the inner wall but not beyond the outer wall, the robot's movement is limited by a rule, where the closer the end moves towards the outer wall, the greater the dragging force is required, inversely, the interaction with the robot is normal. Hence, the restrictions are determined as follows:

$$\begin{cases} x_{evei}(k) = \frac{1}{\exp\left(\frac{|x_{abi}(k-1) - x_{ci}| - |x_{limi} - x_{ci}|}{h}\right)} \cdot x_{thi}(k), & |x_{abi}(k-1) + x_{thi}(k) - x_{limi}| > |x_{abi}(k-1) - x_{limi}| \\ x_{evei}(k) = x_{thi}(k), & |x_{abi}(k-1) + x_{thi}(k) - x_{limi}| < |x_{abi}(k-1) - x_{limi}| \\ \theta_{evei}(k) = \frac{1}{\exp\left(\frac{|\theta_{abi}(k-1) - \theta_{ci}| - |\theta_{limi} - \theta_{ci}|}{h}\right)} \cdot \theta_{thi}(k), & |\theta_{abi}(k-1) + \theta_{thi}(k) - \theta_{limi}| > |\theta_{abi}(k-1) - \theta_{limi}| \\ \theta_{evei}(k) = \theta_{thi}(k), & |\theta_{abi}(k-1) + \theta_{thi}(k) - \theta_{limi}| < |\theta_{abi}(k-1) - \theta_{limi}| \end{cases} \quad (12)$$

where  $x_{abi}(k-1)$  and  $\theta_{abi}(k-1)$  represent the absolute position and the absolute posture of the robot end at moment  $k-1$ , respectively;  $x_{ci}$  and  $\theta_{ci}$  separately represent the midpoint of the virtual inner wall set in position space and posture space;  $x_{limi}$  and  $\theta_{limi}$  are the boundary of the virtual inner wall set in the position space and posture space, which contain the maximum value of the boundary  $x_{maxi}$ ,  $\theta_{maxi}$ , and the minimum value of the boundary  $x_{mini}$ ,  $\theta_{mini}$ ;  $h$  is a parameter applied to regulate mobility.

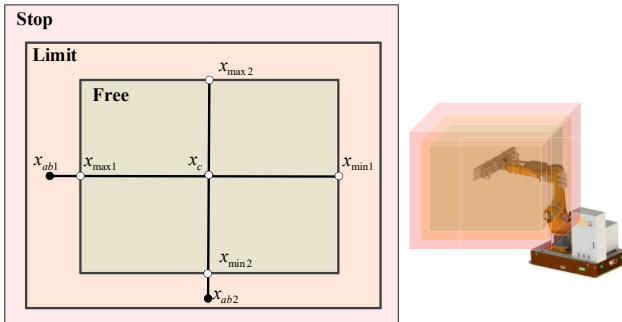


Figure 6. Schematic of virtual walls

When the robot end moves beyond the outer wall,  $x_{evei}(k)$  and  $\theta_{evei}(k)$  are both set to 0, which means the robot is unable to displace no matter how much force is applied.

#### 4. Experiment

The experimental calibrations of each axis of the robot are required to confirm the unstable region before verifying the effectiveness of the admittance control, thus each axis was calibrated individually based on the experimental phenomena discussed in Section 2.2, and then the results are given in Figure 7.

##### 4.1 Simulation results and analysis

To examine the proposed admittance control method, a comparison among different control models is supposed to be made. Since in the literature (Wu *et al.*, 2021), the superiority of Wu's proposed method has been proved by comparing to Lecours *et al.* (2012), the method described in the literature (Wu *et al.*, 2021) is chosen as the reference model in this paper. Then, the comparison among the proposed model, the reference model and the fixed admittance model is provided in this section. Since the simulated force signal ought to reflect the four cases in Section 2.1, the dotted line shown in Figure 8 is generated to imitate the actual manipulation, which contains the phases of gradual force application, constant force dragging, sudden force removal and reverse force application.

**Figure 7.**  
Experimental calibration diagram for each axis of the robot

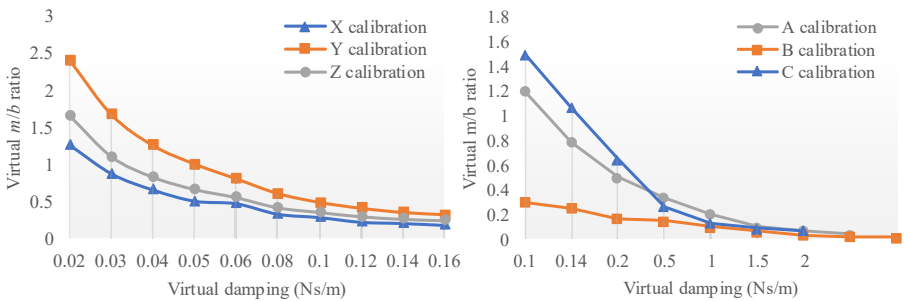
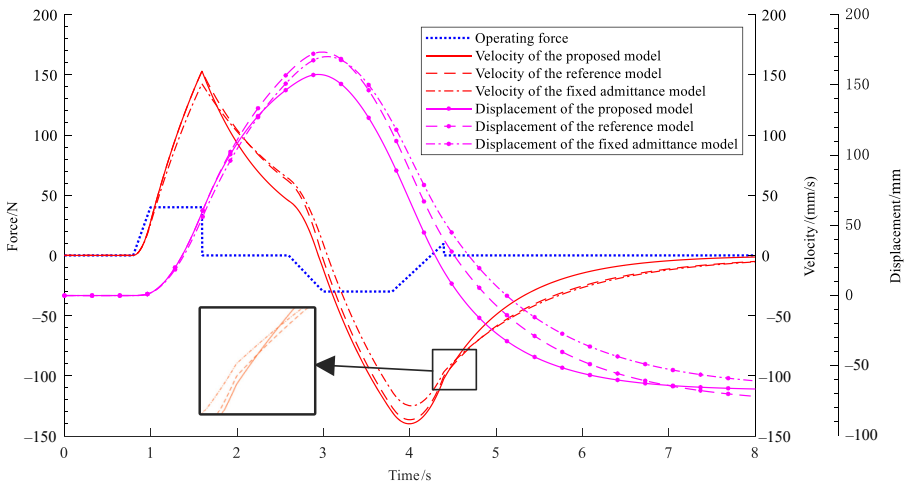


**Figure 8.**  
Simulation comparisons of three admittance control models



Taking the analysis of the  $X$ -axis as an example, the parameters of the three control models are listed in Table 1, which are derived from the stable region. To facilitate inter-model parameter comparisons, the symbols of parameters with the same significance are united across different literature (Wu *et al.*, 2021).

The initial coefficients of the three admittance control models were set in equal, whereas due to the variance of the degree of adaptability, the responses to the same force signal are different. The simulated validation results are shown in Figure 8.

According to Figure 8, it can be seen that:

- (1) In view of the velocity curve, the fixed admittance control method has a slower launching acceleration than the other two control methods in the acceleration phase where the external force is gradually applied, which is unable to reach the desired speed rapidly; in the stopping phase where the force is suddenly unloaded, the proposed method can provide a greater speed reduction than the other two control methods, which enables the robot to respond to cease earlier; besides, the proposed method can reduce the speed faster than the other two methods with a smooth speed transition in the deceleration phase where the force is applied in the reverse direction.
- (2) In view of the displacement curve, the response time of the proposed method to force variation is relatively similar to that of the other two control methods, while it has a higher sensitivity. Particularly, when the external force is removed, applying the proposed method can overcome the inertia effect quicker and stop the motion smoothly without affecting the overall performance, which ensures the safety of the human-robot collaboration process.

#### 4.2 Experimental results and analysis

The robot used for the experiments reported in this paper is the KUKA KR 60 HA industry robot with 6-DOF, and the applied force sensor is the Axia80-M50 sensor from ATI with six dimensions, shown in Figure 9. To imitate the movable airfoils, the prototype is fabricated on a basis weight of 40 kg with a square of  $1.8 \times 0.7$  m, which can also be altered by adding counterweights to change the mass and barycenter. The communication mode between the host computer and the robot is RSI, and the mode between the host computer and the force sensor is UDP, where the communication periods are both 4 ms.

After selecting the parameters in Table 1, the experimental effectiveness of the three models under a common force signal was monitored and output, as shown in Figure 10. Since the existence of small fluctuations in real force signal, the force limitation of  $\pm 10$ N is configured, thus only the excessive force can be imported into the admittance control model.

As can be seen in Figure 10, the proposed admittance control increases the speed by about 15.8% more than the fixed admittance control in the acceleration phase; and in the reversion phase, the proposed control can achieve about 25.0% more dynamic efficiency than the fixed admittance control under same forces; then in the stopping phase, the proposed control can achieve a faster stop than the reference control, saving about 28.8% of the time. Moreover, the robustness of the proposed model facing the presence of small disturbances behaves well.

Fixed admittance model	$m_d = 0.15$ $b_d = 0.12$	/
The reference model	$\lambda_1 = 0.04, \lambda_2 = 0.01,$	$\varepsilon = 0.99$
The proposed model	$\alpha = 0.7, \varphi = 200$	$m_0 = 0.1, \beta = 8, b'_{\min} = 0.05, b'_{\max} = 0.18$

**Table 1.** Parameters of three admittance control models

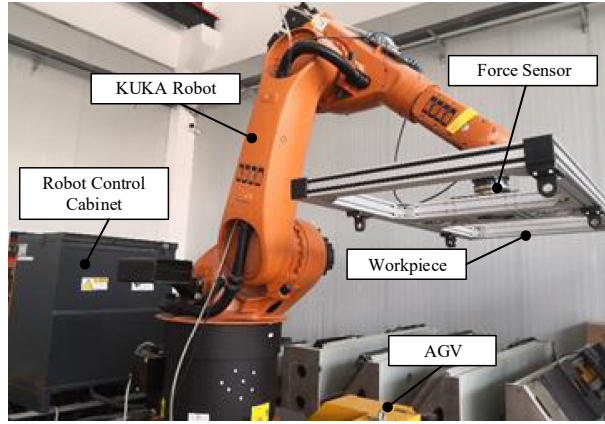


**Figure 9.**  
Schematic of the  
experimental platform

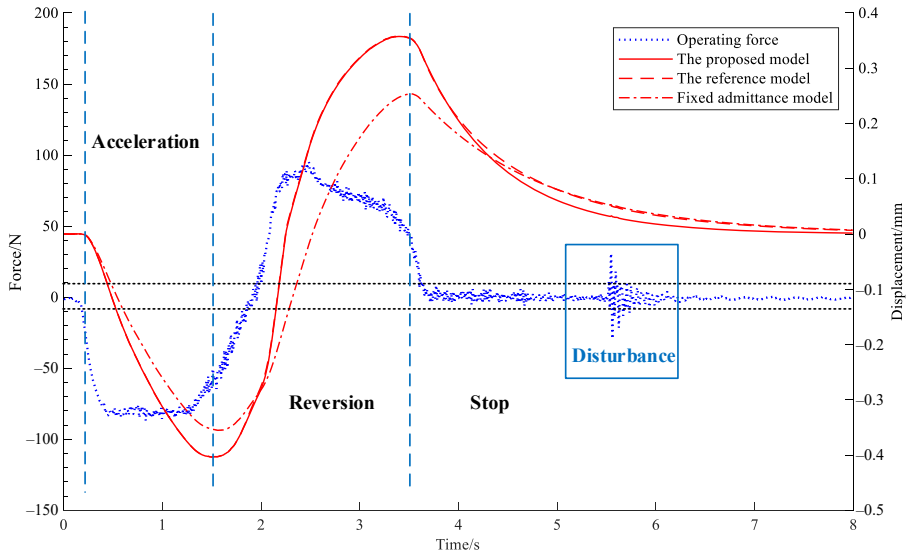


**Figure 10.**  
Experimental  
comparisons of the  
three models

To further verify the robustness of the proposed model, the admittance coefficients located in the unstable region are selected for experiments to demonstrate the consequences of incorrect operation or wrong variation coefficients selection during assembly. The selected initial admittance coefficients are  $m_d = 0.025$ ,  $b_d = 0.05$ , then the performance of each admittance model when encountering the instability is displayed in Figure 11.

Figure 11 shows that when the reference model encounters the condition that the coefficients are located in the unstable region, the treatment of the force-position relation will be out of control, which is liable to cause safety accidents. Moreover, the fixed admittance model has a certain lag, and the low admittance coefficients make the robot move too flexibly, which is not conducive to restraining the influence of inertia. By contrast, the proposed model can still complete the dragging task and can reasonably cope with the situation when the coefficients are mistaken in the unstable domain, which has better robustness.

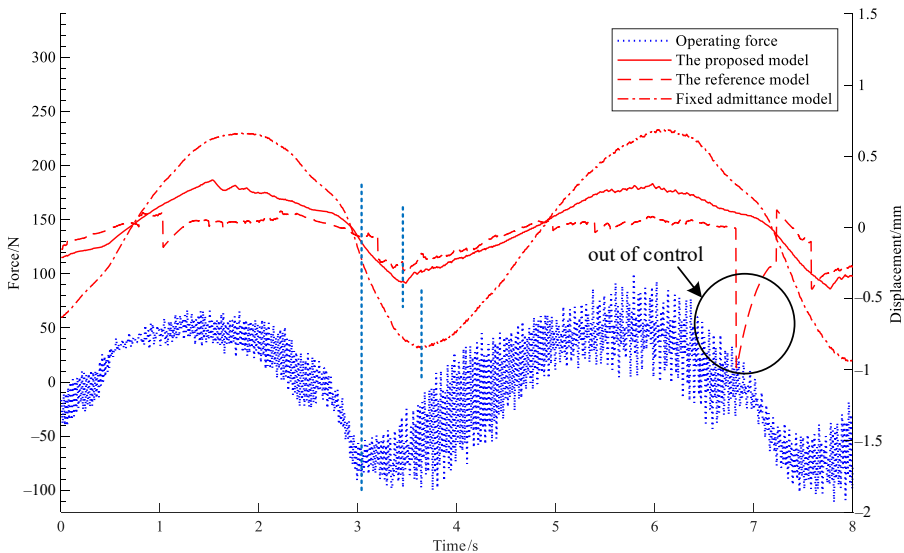


**Figure 11.**  
Performances of  
models under  
instability

## 5. Conclusion

The strategy of human-robot collaboration for the current dilemma of the intelligent assembly of movable airfoils was proposed in this paper. First, a logical judgment of the human's operating intention was constructed. Then, an adaptive admittance control model for suppressing inertial hazards was established, where the rules for selecting the model parameters were elaborated, and the safety and stability issues regarding the assembly process were considered. Finally, simulations and experiments are conducted to compare with other admittance control models. The results show that the inertia hazard can be effectively diminished by adopting the proposed model for the time spent in the stopping phase can be saved at least by about 28.8% compared to other models, and the proposed control model indeed has better robustness.

## References

- Akgun, G., Cetin, A.E. and Kaplanoglu, E. (2020), "Exoskeleton design and adaptive compliance control for hand rehabilitation", Vol. 42 No. 3, pp. 493-502, doi: [10.1177/0142331219874976](https://doi.org/10.1177/0142331219874976).
- Bian, F., Ren, D., Li, R., Liang, P., Wang, K. and Zhao, L. (2020), "Dynamical system based variable admittance control for physical human-robot interaction", *Industrial Robot: An International Journal*, Vol. 47 No. 4, pp. 623-635, doi: [10.1108/IR-12-2019-0258](https://doi.org/10.1108/IR-12-2019-0258).
- Cherubini, A., Passama, R., Crosnier, A., Lasnier, A. and Fraisse, P. (2016), "Collaborative manufacturing with physical human-robot interaction", *Robotics and Computer Integrated Manufacturing: An International Journal of Manufacturing and Product and Process Development*, Vol. 40, pp. 1-13.
- Farhadiyadkuri, F., Popal, A.M., Paiwand, S.S. and Zhang, X. (2022), "Interaction dynamics modeling and adaptive impedance control of robotic exoskeleton for adolescent idiopathic scoliosis", *Computers in Biology and Medicine*, Vol. 145, 105495, doi: [10.1016/j.combiomed.2022.105495](https://doi.org/10.1016/j.combiomed.2022.105495).
- Kim, J. (2022), "Collision detection and reaction for a collaborative robot with sensorless admittance control", *Mechatronics*, Vol. 84, 102811, doi: [10.1016/j.mechatronics.2022.102811](https://doi.org/10.1016/j.mechatronics.2022.102811).

- Lecours, A., Mayer-St-Onge, B. and Gosselin, C. (2012), "Variable admittance control of a four-degree-of-freedom intelligent assist device", *paper presented at the IEEE International Conference on Robotics & Automation*.
- Li, B., Tian, W., Zhang, C., F., Hua, F., F., Cui, G., Y. and Li, Y., F. (2022), "Positioning error compensation of an industrial robot using neural networks and experimental study", *Chinese Journal of Aeronautics*, Vol. 35 No. 2, pp. 346-360.
- Lv, Q., Zhang, R., Liu, T., Zheng, P., Jiang, Y., Li, J., Bao, J. and Xiao, L. (2022), "A strategy transfer approach for intelligent human-robot collaborative assembly", *Computers and Industrial Engineering*, Vol. 168, 108047, doi: [10.1016/j.cie.2022.108047](https://doi.org/10.1016/j.cie.2022.108047).
- Peng, Y., Chen, S., Jivani, D., Wason, J. and Wen, J.T. (2021), "Sensor-guided assembly of segmented structures with industrial robots", *Applied Sciences*, Vol. 11 No. 6, p. 2669.
- Pérez, L., Rodríguez-Jiménez, S., Rodríguez, N., Usamentiaga, R. and Wang, L. (2020), "Symbiotic human-robot collaborative approach for increased productivity and enhanced safety in the aerospace manufacturing industry", *The International Journal of Advanced Manufacturing Technology*, Vol. 106 Nos 3-4, pp. 1-13.
- Rojas-García, L.N., Chávez-Olivares, C.A., Bonilla-Gutiérrez, I., Mendoza-Gutiérrez, M.O. and Ramírez-Cardona, F. (2022), "Force/position control with bounded actions on a dexterous robotic hand with two-degree-of-freedom fingers", *Biocybernetics and Biomedical Engineering*, Vol. 42 No. 1, pp. 233-246, doi: [10.1016/j.bbe.2021.12.006](https://doi.org/10.1016/j.bbe.2021.12.006).
- Tsumugiwa, T., Yokogawa, R. and Hara, K. (2017), "Variable impedance control based on estimation of human arm stiffness for human-robot cooperative calligraphic task", *paper presented at the IEEE International Conference on Robotics & Automation*.
- Wu, C., Shen, Y., Li, G., Li, P. and Tian, W. (2021), "Compliance auxiliary assembly of large aircraft components based on variable admittance control", *paper presented at the Intelligent Robotics and Applications, Cham*.
- Yang, C., Wu, Y., Ficuciello, F., Wang, X. and Cangelosi, A. (2021), "Guest editorial: special issue on human-friendly cognitive robotics", *IEEE Transactions on Cognitive and Developmental Systems*, Vol. 13 No. 1, pp. 2-5, doi: [10.1109/TCDS.2020.3044691](https://doi.org/10.1109/TCDS.2020.3044691).

**Corresponding author**

Wei Tian can be contacted at: [tw\\_nj@nuaa.edu.cn](mailto:tw_nj@nuaa.edu.cn)